

High-resolution optical spectroscopy in a hollow-core photonic crystal fiberC. Perrella,¹ P. S. Light,¹ T. M. Stace,² F. Benabid,³ and A. N. Luiten¹¹*Department of Physics, University of Western Australia, Perth, Western Australia 6009, Australia*²*ARC Centre of Excellence in Engineered Quantum Systems, University of Queensland, Brisbane, Queensland 4072, Australia*³*Centre for Photonics and Photonic Materials, University of Bath, Bath BA2 7AY, United Kingdom*

(Received 1 July 2011; published 25 January 2012)

In this paper, we present detailed high-resolution spectroscopy of rubidium (Rb) vapor confined within a hollow-core photonic crystal fiber (HC-PCF). We find a very low level of additional frequency broadening associated with this confinement, with spectral features being only 1 MHz broader than the natural linewidth of the excited state. We show that this additional broadening is consistent solely with the atoms' transit across the fiber's optical mode. This low level of decoherence opens the door to a wide variety of applications including compact frequency standards and new types of quantum optical devices based on alkali-metal-loaded HC-PCFs. We highlight the low level of decoherence through observation of electromagnetically induced transparency in the confined vapor.

DOI: [10.1103/PhysRevA.85.012518](https://doi.org/10.1103/PhysRevA.85.012518)

PACS number(s): 32.30.-r, 42.81.Qb, 78.47.da, 78.47.nd

I. INTRODUCTION

A recent innovation in photonics is the development of hollow-core optical fibers that simultaneously confine vapors and guide light within their cores over large distances [1]. This capability has attracted great interest for applications in frequency stabilization [2,3], electromagnetically induced transparency (EIT) [4–6], slow light [7], few-photon optical switches [8], and deterministic quantum logic gates [9]. However, the full potential of this strong light-atom interaction can only be realized if the deleterious effects of fiber-atom interaction can be minimized.

Previous work utilizing vapors [10,11] in hollow-core photonic crystal fiber (HC-PCF) has shown large dephasing effects caused by transit time [3,10,12] or pressure broadening [2,6,7]. Such effects limit this technology in applications where optical coherences play a key role.

Here we report a very low dephasing rate (~ 1 MHz) within HC-PCF, which opens the door to a wide range of applications. This was achieved in untreated silica fiber loaded with rubidium (Rb) vapor. We show that small residual broadening effects are consistent with finite light-atom interaction time. We also explain our observation that the Rb vapor exhibits greatly increased saturation intensity in this geometry compared to that in a conventional cell.

Using the optical setup shown in Fig. 1, we investigated dephasing and decay processes of Rb vapor confined to the fiber core and in a reference bulk cell. Via direct fluorescent decay measurements and the saturation behavior of spectral features, we measured the influence of finite interaction time on the atomic population dynamics. Finally, we demonstrate how the low level of decoherence enables creation of highly efficient EIT. These observations are consistent with a four-level atomic model, which we discuss.

II. SETUP

We used kagome-lattice [13] HC-PCF with a single-cell core defect of diameter $45 \mu\text{m}$ (see Fig. 1). This fiber exhibits low-loss guidance from 600 to 1600 nm. Each end of the 40-cm fiber was held in separate vacuum chambers while the midsection was outside the vacuum system. Each chamber had

windows to couple light into the fiber and to allow monitoring of Rb vapor densities within the vacuum chambers.

The whole vacuum system, including fiber and chambers, was outgassed at 100°C , achieving pressures below 10^{-7} Torr measured at the ion pump. Rubidium was released into one chamber from a Rb ampoule at these elevated temperatures producing high Rb vapor densities and promoting diffusion into the fiber from the vacuum chamber's high-pressure environment. Observation of Rb fluorescence scattered out the side of the fiber indicates that over half its length was filled after four months of loading. On-resonance transmission of the ^{85}Rb D_2 transition through the fiber showed an absorption coefficient $\alpha L \sim 10$. We believe this slow filling rate is associated with Rb atoms coating and pacifying the fiber core surface. After the initial load, we were able to recover the original optical depth in ~ 2 days by returning the vacuum system to the loading conditions specified above. Rb vapor was observed within the fiber from 20°C to 120°C with the density strongly dependent on the fiber temperature. For the experiments discussed below, the temperature of the vacuum system was lowered to 60°C to avoid extinction of the laser beam on resonance.

Two lasers were used to conduct hole-burning spectroscopy within the fiber and bulk cell: the pump was an intense Ti:sapphire laser tuned to the 795-nm D_1 transition, while the probe was a tunable extended-cavity diode laser (ECDL), which scanned through the 780-nm D_2 transition. In order to measure frequencies precisely, part of the probe laser was directed to an optical cavity and a saturated absorption spectrometer. The resonances of the optical cavity provided equally spaced frequency markers with a free spectral range (FSR) of ~ 300 MHz. The absolute frequency of the probe and an accurate estimation of the optical cavity's FSR were obtained using the known spacings between several of the saturated absorption features. These elements provided a frequency axis with an accuracy of 2%.

A chopper wheel or an acousto-optic modulator (AOM) enabled independent amplitude modulation of the lasers, which were combined on a polarization beam splitter as shown in Fig. 1. The combined beam was focused into the fiber core and also sent to a Rb cell. The $1/e^2$ intensity beam diameters

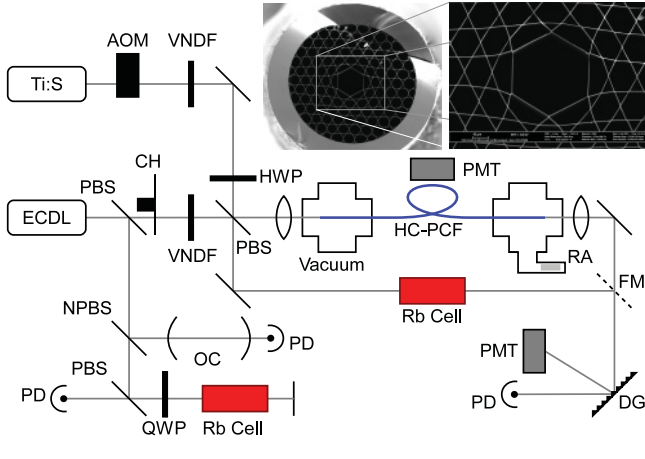


FIG. 1. (Color online) Schematic of the optical experimental setup. HWP (QWP), half (quarter) wave plate; NPBS (PBS), nonpolarizing (polarizing) beam splitter; CH, chopper wheel; AOM, acousto-optic modulator; OC, optical cavity; VNDF, variable neutral density filter; RA, rubidium ampoule; FM, flip mirror; DG, diffraction grating; PD, photodiode; and PMT, photomultiplier tube. Inset, top right: scanning electron microscope image of the kagome HC-PCF cross section.

for the fiber and cell were $36 \mu\text{m}$ and 2 mm , respectively. After the fiber or cell, the pump and probe beams were separated using a diffraction grating, detected by either a photomultiplier tube (PMT) or photodiode, and then demodulated using a lock-in amplifier. Typical spectra obtained from the fiber are shown in Fig. 2(a).

III. BROADENING PROCESSES

For the remainder of this paper, we primarily consider the ^{87}Rb isotope and its D_1 and D_2 transitions. We denote the two $5S_{1/2}$ ground states as $|g_F\rangle$, where $F = 1, 2$ labels the total atomic angular momentum quantum number. Similarly, we denote the $5P_{1/2}$ excited state manifold as $|a_F\rangle$ and the $5P_{3/2}$ manifold as $|b_F\rangle$, where the subscripts label the hyperfine states of each manifold. This labeling convention is shown in Fig. 2(b).

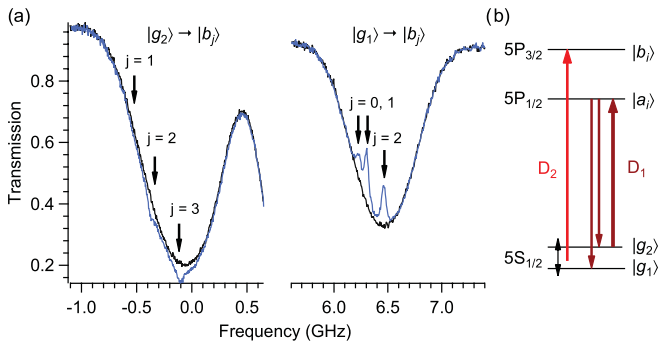


FIG. 2. (Color online) (a) Transmission spectra of the Rb-filled fiber on the ^{87}Rb D_2 transitions with (blue) and without (black) the pump laser. The frequency axis is detuned from the ^{87}Rb $g_2 \rightarrow b_3$ transition. Arrows indicate the position of the pumped features. (b) An energy-level diagram showing the pump tuned to the D_1 transition and probe tuned to the D_2 transition.

To measure the broadening processes within the fiber, we used hole-burning spectroscopy, which avoids Doppler broadening effects. The Ti:sapphire laser was tuned to the D_1 transition to perturb the thermal equilibrium characteristics of the ground states. The resulting disturbance was measured with the ECDL, as it scanned across the D_2 transitions. With the Ti:sapphire laser resonant with the $|g_1\rangle \rightarrow |a_2\rangle$ transition, we observed spectral holes in the $|g_1\rangle \rightarrow |b_j\rangle$ set of transitions while also observing excess population features in the $|g_2\rangle \rightarrow |b_j\rangle$ transition [see Fig. 2(a)]. We observed three holes and three corresponding peaks due to the three excited-state hyperfine transitions in the D_2 Doppler-broadened resonances. We used two-color hole-burning spectroscopy rather than conventional saturation spectroscopy to avoid complications arising from optical interference and Zeeman pumping effects, which make interpretation of saturation spectroscopy features very complex.

To extract the linewidth of the resulting features, we fit the probe absorption spectrum with the form [14]

$$\exp \left\{ -\frac{\alpha_{ij}}{\mu_{ij}} \left(1 + \frac{h_{ij}\Gamma_{ij}^2}{\Gamma_{ij}^2 + 4\Delta_{ij}^2} \right) \exp \left[-\frac{1}{2} \left(\frac{\Delta_{ij}}{\Delta_{\text{Dop}}} \right)^2 \right] \right\}, \quad (1)$$

where α_{ij} and μ_{ij} are the $|g_i\rangle \rightarrow |b_j\rangle$ transition absorption coefficient and spectroscopic strength factor [15], respectively, Γ_{ij} and h_{ij} are the width and fractional height of the burnt hole (or excess population feature) respectively, $\Delta_{ij} = \omega_L - \omega_{ij}$ is the laser detuning, and Δ_{Dop} is the Doppler absorption width. Varying the pump power yields the power dependence of the linewidth, Γ_{ij} , and the result is shown in Fig. 3(a).

The driven system was modelled using a simple four-level atomic model, consisting of the two excited states, $|a_j\rangle$ and $|b_j\rangle$, and the two ground states, $|g_1\rangle$ and $|g_2\rangle$. States $|g_1\rangle$ and $|a_j\rangle$ were coupled by a pump laser with Rabi frequency, $\Omega_p(t)$,

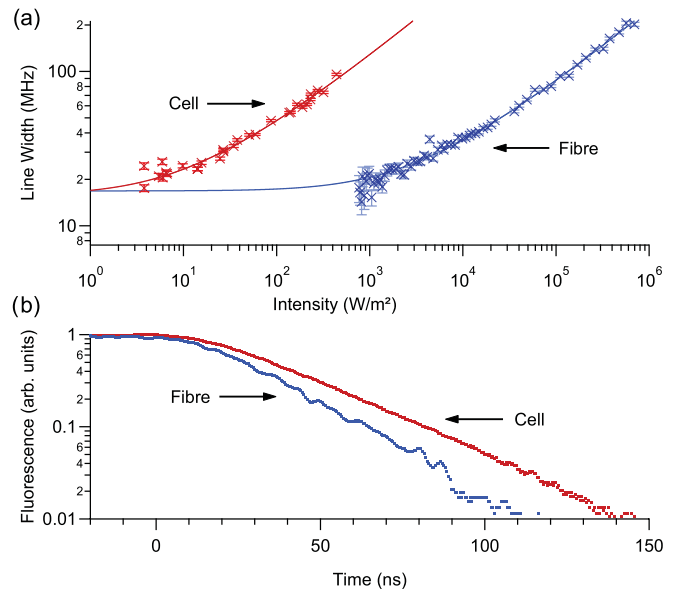


FIG. 3. (Color online) (a) The intensity dependence of the linewidth of the hole-burn features for the fiber and a bulk cell. The solid lines are theoretical fits to the data. (b) Fluorescence decay measurements of both the fiber and cell.

while a probe laser of strength $\Omega_s(t)$ was scanned across the resonances $|g_1\rangle \leftrightarrow |b_j\rangle$ and $|g_2\rangle \leftrightarrow |b_j\rangle$. The excited states decayed into the ground-state manifold with known branching ratios [16]. The evolution of a particular atom crossing the beam is governed by the master equation

$$\begin{aligned} \dot{\rho} &= -i[H, \rho] + \sum_{g_i} \Gamma_{g_i}^{a_j} \mathcal{D}[|a_j\rangle\langle g_i|]\rho + \Gamma_{g_i}^{b_j} \mathcal{D}[|b_j\rangle\langle g_i|]\rho, \\ H &= (\omega_{b_j} - \omega_s)|b_j\rangle\langle b_j| + (\omega_{a_j} - \omega_p)|a_j\rangle\langle a_j| + \omega_{g_2}|g_2\rangle\langle g_2| \\ &\quad + (\Omega_s(t)|b_j\rangle\langle g_1|/2 + \Omega_p(t)|a_j\rangle\langle g_1|/2 + \text{H.c.}), \end{aligned} \quad (2)$$

where $|\tilde{g}\rangle = |g_1\rangle + |g_2\rangle$ [17]. Absorption of the probe is then proportional to $\text{Im}[\Omega_s \langle \tilde{g} | \rho | b_j \rangle]$. Atoms with different speeds and trajectories will see different time-dependent pump and probe fields. To account for this, we averaged the absorption over the Maxwell-Boltzmann distribution similar to that presented in Ref. [18]. In a pump-probe experiment of this type, the absorption spectrum of the probe laser will be affected by both the pump-induced Rabi splitting [14] and transit-time-broadened Voigt profile [15]. Our calculations show that both of these effects are obscured by the distribution of atomic trajectories, resulting in a line shape that is close to Lorentzian.

The model was solved numerically, showing that Γ_{ij} varies with intensity with a form given by

$$\Gamma(I) = \Gamma_{D_1} \sqrt{1 + I/(2I_{\text{Sat}})} + \Gamma_{D_2} + \Gamma_{\text{trans}}, \quad (3)$$

where Γ_{D_1} and Γ_{D_2} are the “zero-power” linewidths of the pump and probe transitions, Γ_{trans} is the transit time broadening, and I_{Sat} is a phenomenological saturation parameter. Fitting Eq. (3) to experimental data and extrapolating to zero intensity gives FWHM linewidths of the features within the fiber of 16.8 ± 0.4 MHz and 15.9 ± 0.6 MHz for the cell.

The factors contributing to the “zero-power” widths are summarized in Table I. The linewidths of the lasers were estimated from the frequency noise inferred from intensity noise on the side of a Rb D_2 resonance. The ECDL Voigt linewidth was 2.55 MHz, consisting of Lorentzian and Gaussian components of 966 kHz and 1.74 MHz respectively. The Ti:sapphire Lorentzian linewidth was 62 kHz. These linewidths were convolved with the atomic linewidths to give the broadening in Table I. Ambient magnetic fields contributed a further 2.0 ± 0.5 MHz broadening to both the fiber and cell spectra, as estimated by comparison of saturated spectra in the cell

TABLE I. Zero-power hole broadening budget.

Effect	Contribution (MHz)
D_1 natural linewidth [16]	5.75
D_2 natural linewidth [16]	6.07
Laser linewidth (Lorentzian component)	1.03 ± 0.07
Laser linewidth (Gaussian component)	1.74 ± 0.07
Zeeman splitting	2.0 ± 0.5
Resultant	15.3 ± 0.5
Cell experimental value	15.9 ± 0.6
Fiber experimental value	16.8 ± 0.4
Additional fiber broadening	1.0 ± 0.7
Transit-time broadening (theory)	0.44

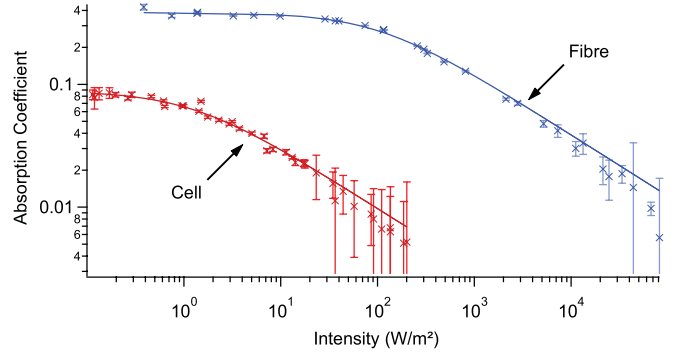


FIG. 4. (Color online) Optical depth of the fiber and cell as a function of intensity. Solid lines are fits to Eq. (4).

with and without magnetic shields. In total, the fiber exhibits a “zero-power” linewidth 1.0 ± 0.7 MHz broader than that of the cell. This is consistent with a predicted transit-time broadening of 0.44 MHz calculated using our four-level atomic model.

To confirm these conclusions, we also measured fluorescence decay rates. The Ti:sapphire laser was tuned to the ^{85}Rb $g_2 \rightarrow a_{2,3}$ transitions and an AOM was used to extinguish the light in 7 ns. A PMT detected scattered light from the Rb vapor in the fiber and the cell. Figure 3(b) shows the average of 4000 of these decay measurements. The fiber lifetime was 21.7 ± 1.7 ns, and that in the cell was 27.8 ± 0.7 ns. The cell measurement is consistent with previous measurements of the D_2 lifetime [16], while the reduced lifetime in the fiber is associated with quenching of excited state through collisions with the fiber wall. This is in good agreement with the model prediction of an average atomic lifetime within the fiber of 22.9 ± 0.2 ns.

IV. OPTICAL SATURATION

There is a large difference in the effective saturation intensity between the cell and fiber measurements in Fig. 3(a). To understand this in more detail, we measured the optical saturation behavior of the $D_1, |g_1\rangle \rightarrow |a_2\rangle$ Doppler-broadened transition for which the hyperfine energy levels of this excited state are fully resolved. This is shown in Fig. 4 for both the fiber and cell, together with a theoretical fit based on the expected saturation form of the absorption [14]:

$$\alpha(I) = \alpha_0 / \sqrt{1 + I/I_{\text{Sat}}}, \quad (4)$$

where α_0 is the “zero-power” optical depth, I is the probe laser’s intensity, and I_{Sat} is the fitted saturation intensity. We find $I_{\text{Sat}}^{(\text{cell})} = 1.2 \pm 0.1$ W/m², while $I_{\text{Sat}}^{(\text{fiber})} = 102 \pm 7$ W/m², which is a factor of ~ 85 times larger than $I_{\text{Sat}}^{(\text{cell})}$ and a factor of 2 above the two-level saturation intensity of 53.9 W/m² for this transition [16].

Ordinarily, optical saturation originates from optical pumping into uncoupled ground states. In the fiber case, the short transit time means that pumping is substantially reduced, leading to a much higher saturation intensity. A model for the saturation behavior of an open effusive atomic system crossing a Gaussian laser beam in time t has been previously presented in Ref. [19]. The degree of optical pumping is

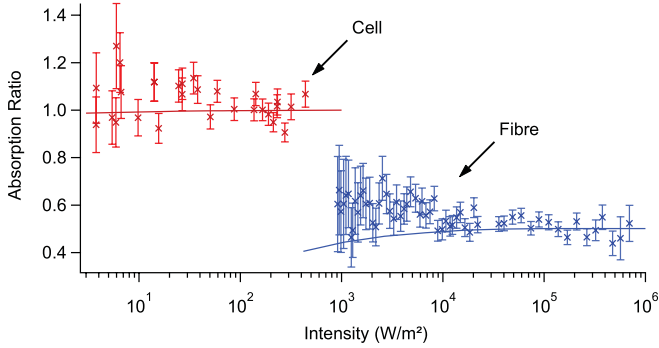


FIG. 5. (Color online) Absorption transfer ratio, \mathcal{R}_i , for the fiber and a bulk cell as a function of intensity. Solid lines are predictions from the numerical model described by Eq. (2).

characterized by a parameter \mathcal{F} , which is an estimate of the pump-induced population transfer: $\mathcal{F} = 0$ represents no perturbation to the thermal equilibrium situation, while $\mathcal{F} = 1$ represents complete population transfer to the uncoupled ground state (and thus complete transparency). The condition $\mathcal{F} \sim 0.5$ corresponds to $I = I_{\text{Sat}}$. For an atomic transit time t , and when the population transfer is small, \mathcal{F} takes the form [19]

$$\mathcal{F} = \begin{cases} (\Omega_p t/2)^2 & \Gamma t \ll 2 \\ \Omega_p^2 t/(2\Gamma) & \Gamma t \gg 2, \end{cases} \quad (5)$$

Both fiber and the cell are in the regime $\Gamma t > 2$, where the perturbation to the ground state is proportional to both the pump power and the transit time. Therefore, the ratio of the saturation powers should be approximately the inverse of the ratio of the transit times for the two cases. In our case, $t^{(\text{cell})}/t^{(\text{fiber})} \approx 60$, while $I_{\text{Sat}}^{(\text{fiber})}/I_{\text{Sat}}^{(\text{cell})} = 85$, which are in reasonable agreement given that Eq. (5) is only valid for small \mathcal{F} and ignores the distribution of transit times.

V. ELECTROMAGNETICALLY INDUCED TRANSPARENCY

A final deep insight into the effect of the pump on the probe transmission can be gained by comparing the magnitude of the spectral hole features seen in the $|g_1\rangle \rightarrow |b_j\rangle$ manifold to that of the peak features seen in the $|g_2\rangle \rightarrow |b_j\rangle$ manifold (see Fig. 2).

The ratio of hole-to-peak heights, $\mathcal{R}_i = -h_{2i}/h_{1i}$, in Eq. (1) yields an absorption ratio, which will be 1 if the entire population from one ground state had been transferred to the other ground state. A ratio of less than unity indicates that the optical saturation behavior cannot simply be explained by population transfer between ground states.

Figure 5 shows \mathcal{R}_i for both the fiber and cell. We find $\mathcal{R}_i^{(\text{cell})} = 1.02 \pm 0.08$ and $\mathcal{R}_i^{(\text{fiber})} = 0.53 \pm 0.06$, independent

of both intensity and i . Also shown are solid lines calculated from the four-level atomic model, which are in close agreement with the experimental data.

In this cell, the transit time is long enough that all excited-state population decays to the other ground state, and hence the ratio is essentially unity. In the fiber, the ratio is approximately 0.5, so population transfer alone is not sufficient to explain the apparent decrease in absorption from the pump-coupled ground state. The physical origin for the lower ratio in the fiber lies in the much higher intensities in the fiber together with a transit time comparable to the lifetime of the excited state. The short transit time and strong coherent driving of the pump laser lead to a substantial Rabi splitting of the coupled ground state. The increased transparency of the vapor is therefore explained by EIT. The probe and pump together form a V configuration for EIT, which is absent when the probe is tuned to the $|g_2\rangle \rightarrow |b_j\rangle$ [20]. Since $t^{-1} \sim \Gamma \ll \Omega_p$ implies that neither the dephasing effects of decay nor the masking effects of optical pumping can hide EIT, as they usually do in the V configuration, the effect of EIT in the fiber is substantial. Our model indicates that EIT accounts for half the hole depth seen in the $|g_1\rangle \rightarrow |b_j\rangle$ transitions. It is the action of this EIT peak that results in \mathcal{R} approaching 0.5 at the highest intensities.

VI. CONCLUSIONS

We have demonstrated that a Rb-filled HC-PCF can show narrow spectral features that are only ~ 1 MHz broader than the natural atomic linewidth. This additional broadening arises solely from coherent transit-time effects and can thus be further reduced with larger core fibers. The absence of any additional dephasing supports the potential for use of this technology in miniature, robust clocks and quantum optics experiments. Measurements of the fluorescent decay time of fiber-confined atoms directly demonstrates the influence of the walls on the excited-state lifetime of the atoms. Finally, in contrast to the usual observation in cells, we observed a saturation intensity of the atoms in the fiber that is of the same order as the value expected from a simple two-level model [16]. The small influence of optical pumping and the low level of decoherence are confirmed by the demonstration of EIT in the fiber confined atoms.

ACKNOWLEDGMENTS

The authors acknowledge financial support from the Australian Research Council. We also acknowledge Francois Couny for fabricating the HC-PCF and the Australian Microscopy and Microanalysis Research Facility at the University of Western Australia, a facility funded by the university and state and commonwealth governments.

- [1] F. Benabid and P. J. Roberts, *J. Mod. Opt.* **58**, 87 (2011).
 [2] K. Knabe *et al.*, *Opt. Express* **17**, 16017 (2009).
 [3] J. Hald, J. C. Petersen, and J. Henningsen, *Phys. Rev. Lett.* **98**, 213902 (2007).
 [4] P. S. Light *et al.*, *Opt. Lett.* **32**, 1323 (2007).

- [5] S. Ghosh, A. R. Bhagwat, C. K. Renshaw, S. Goh, A. L. Gaeta, and B. J. Kirby, *Phys. Rev. Lett.* **97**, 023603 (2006).
 [6] F. Benabid *et al.*, *Opt. Express* **13**, 5694 (2005)
 [7] S. Ghosh, J. E. Sharping, D. G. Ouzounov, and A. L. Gaeta, *Phys. Rev. Lett.* **94**, 093902 (2005).

- [8] M. Bajcsy, S. Hofferberth, V. Balic, T. Peyronel, M. Hafezi, A. S. Zibrov, V. Vuletic, and M. D. Lukin, *Phys. Rev. Lett.* **102**, 203902 (2009).
- [9] J. D. Franson, B. C. Jacobs, and T. B. Pittman, *Phys. Rev. A* **70**, 062302 (2004).
- [10] A. D. Slepkov, A. R. Bhagwat, V. Venkataraman, P. Londero, and A. L. Gaeta, *Phys. Rev. A* **81**, 053825 (2010).
- [11] A. M. Cubillas *et al.*, *Opt. Express* **16**, 3976 (2008).
- [12] K. Saha, V. Venkataraman, P. Londero, and A. L. Gaeta, *Phys. Rev. A* **83**, 033833 (2011).
- [13] F. Couny *et al.*, *Opt. Lett.* **31**, 3574 (2006).
- [14] S. C. Rand, *Lectures on Light: Nonlinear and Quantum Optics Using the Density Matrix* (Oxford University Press, Oxford, 2010).
- [15] W. Demtröder, *Laser Spectroscopy*, 3rd ed. (Springer-Verlag, Berlin, Germany, 2003).
- [16] D. A. Steck, *Rubidium 87 D Line Data*, available at [<http://steck.us/alkalidata>].
- [17] D. F. Walls and G. J. Milburn, *Quantum Optics* (Springer-Verlag, Berlin, Germany, 2008).
- [18] T. M. Stace and A. N. Luiten, *Phys. Rev. A* **81**, 033848 (2010).
- [19] G.-W. Truong, E. F. May, T. M. Stace, and A. N. Luiten, *Phys. Rev. A* **83**, 033805 (2011); **85**, 019909(E) (2012).
- [20] D. J. Fulton, S. Shepherd, R. R. Moseley, B. D. Sinclair, and M. H. Dunn, *Phys. Rev. A* **52**, 2302 (1995).